Uniport Journal of Engineering and Scientific Research (UJESR)

Vol. 6, Issue 2, 2022, Page 189-203
ISSN: 2616-1192

(www.ujesr.org)

Computational Study of Heat Transfer and Entropy Generation in Novel M-Like Structure Microchannel Heat Sink using TiO_2 Nanofluid

Fetuga, I.A, Olakoyejo, O.T*, Oluwadare, S.R, Oluwatusin, O and Adelaja, A.O
Department of Mechanical Engineering, University of Lagos, Akoka, Lagos, Nigeria.
*Corresponding author's email: oolakoyejo@unilag.edu.ng

Abstract
In this work, ANSYS FLUENT software was employed to conduct a numerical analysis of the heat transfer characteristics and entropy generation rate of a TiO_2 nanofluid in a novel M-like structure microchannel heat sink (MCHS) which was subjected to a steady-state flow and constant heat flux. The three-dimensional simulation was carried out for various Reynolds numbers (100–750) and nanoparticle concentrations (0.25% to 2%) for a varied microchannel height of 200 μm to 500 μm. The effects of heat transfer characteristics (Nusselt number), entropy generation rate (thermal, $S'_{gen\ th}$ and frictional, $S'_{gen\ fr}$), and entropy generation number ratios ($N_{s,nf}/N_{s,f}$) of nanofluids on MCHS were investigated. From the results, it was reported that increasing microchannel height (H) from 200 μm to 500 μm yielded an increase in Nusselt number of about 6.77%-57% and a reduction of about 99%-75% for frictional entropy generation rate. Meanwhile, a decrease in microchannel height from 500 μm to 200 μm caused a reduction of about 77.5%-26.8% for thermal entropy generation rate. It was also observed that augmenting the volume fraction of TiO_2 nanoparticles from 0.25% to 2% caused an enhancement in heat transfer from 30% to 98.9%, a decrease of 33.3%-1.85% for thermal entropy generation rate, and an increment of 2.22%–26.5% for frictional entropy generation rate. Furthermore, the results revealed that it is not thermodynamically advisable to employ nanofluids at H=200 μm because it is dominated by pressure drop, whereas at H=500 μm and at Re≤400, the heat sink will perform better under this condition.

Keywords: *Computational fluid dynamics, Microchannel heat sink, Nanofluid, Entropy generation, Friction factor, Nusselt number, Volume fraction*

Received: 28th June, 2022 *Accepted: 2nd August, 2022*

1. Introduction

It is widely known that microelectronic technologies make electronic devices less bulky and compact. However, the increased overall density of chips and miniaturization of electronic packages poses a danger of lower efficiency and high heat accumulation within an electronic device. Therefore, thermal management is critical for maximizing efficiency and extending the lifespan of microelectronic devices. During the last few years, many cooling strategies have been on how to fulfil the high heat dissipation rate requirements while maintaining a low junction temperature. The use of a microchannel heat sink (MCHS) is one of these attempts due to its capacity to create a high heat transfer coefficient, compact dimension and volume per heat load, and low coolant needs.

The cooling concept of MCHS was first propounded by Tuckerman and Pease (1981). Since then, the performance of MCHS with various nanoparticle materials and geometry parameters has been intensively researched over the last two decades. A study on the development of MCHS was conducted by Kandlikar et al. (2003). The MCHS has a vast number of parallel microchannels varying in hydraulic diameter from 10 to 1000 μm to cool the heated medium, and a coolant was applied through the entry region of the channels. Although the MCHS can enhance thermal performance, additional advancements are required to fulfil the growing needs of diverse electronic device applications. From the thermal engineering perspective, the heat transfer properties of the MCHS are improved by increasing its thermal performance. Hence, improving heat transfer performance requires strategies for enhancing

MCHS heat transfer efficiency. This goal can be accomplished in a variety of ways.

Firstly, it is required to increase the thermophysical characteristics of the working fluid, which may be done by adding nanofluids to the base fluid. This involves introducing specific amounts of nanoparticles with better thermal conductivity into the base fluid. Choi and Eastman (1995) from Argonne National Laboratory were the first to suggest nanofluids by employing nanofluid as a suspension. They discovered that the thermal conductivity of nanofluids improved substantially. Lee et al. (1999) showed that an ethylene glycol containing 4.0 percent of CuO particles increases thermal conductivity by 20%. (Koo et al., 2005; Jang and Choi, 2006) used several models for the effective thermal conductivity of nanofluids to investigate the performance of MCHS numerically. Chein and Hunag (2005) adopted a macro-scale heat transfer coefficient correlation to predict the performance of a microchannel heat sink. Chein and Chuang (2007) experimentally investigated the influence of nanofluid on the performance of MCHS. They concluded that the thermal conductivity of the nanoparticles might improve the heat transfer coefficient in a laminar flow situation. Das et al. (2003) examined the influence of thermal conductivity of nanofluids on MCHS. They revealed that a temperature range of 21–51°C improves the thermal conductivity of nanofluid by 2-4 times. Yang et al. (2005) experimentally studied the heat transfer characteristics of nanofluids in a microchannel under a laminar flow condition. They concluded that the heat transfer coefficient for the nanofluid flow had a smaller increase than obtained by either the conventional heat transfer correlation for the homogeneous or particle-suspended fluid.

The second way to achieve a better-performed MCHS is to reduce the irreversibility of the system Ibáñez et al. (2013). The measured degree of irreversibility in a thermal system is known as entropy generation, and it helps determine the efficacy of the thermal system. In a thermal system, entropy generation can be employed as an optimization method if the objective is directed towards effective minimization. Yang et al. (2015) studied the entropy generation optimization of a nanofluid flowing through a trapezoidal microchannel using numerical simulations. Because the temperature difference between the fluid and the wall was substantial and the trapezoidal microchannel generated a thermal entropy nearly three times greater than the frictional effects, the maximum thermal entropy generation rate was attained towards the bottom and side walls. Shalchi et al. (2012) numerically investigated the entropy generation and convective heat transfer of Al_2O_3 nanofluid flowing tangentially in a microchannel heat sink. They discovered that when the particle volume fraction and Reynolds number of nanoparticles increased, the entropy generation rate decreased. Hassan et al. (2013) used a numerical approach to examine the entropy generation of flowing nanofluids in mini and microchannels, utilizing two different thermal conductivity and viscosity models. They concluded that in a laminar flow regime, Al_2O_3 nanoparticles enhanced the overall entropy generation rate at a significantly higher rate than the base fluid. Thus, Al_2O_3 nanofluids were reported to be unsuitable for microchannels usage; nevertheless, a small increase in entropy production rate over the base fluid was obtained for mini-channels. Bianco et al. (2014) examined the turbulent convective heat transfer in a mini-channel at constant wall temperature. Nanofluids were found to transfer heat more efficiently than pure water while also causing a slight pressure decrease. Ebrahimi et al. (2016) researched entropy generation using Al_2O_3 and CuO water nanofluid in a microchannel incorporated with vortex generators. When compared to the base fluid, they reported that nanofluids reduced irreversibility. Ting et al. (2016) looked into the impacts of dissipation on the entropy generation of Al_2O_3-water nanofluids in a microchannel heat sink and revealed that the rise in frictional irreversibility was responsible for the relatively high entropy generation rate.

The third approach to obtaining better MCHS performance is either by increasing the flow velocity or enlarging the contact area of the channel. The microchannel's geometry greatly influences the fluid's velocity and the contact area. Chen et al. (2007) demonstrated that channel aspect ratios are responsible for velocity and fluid temperature distribution. Therefore, numerous researchers have looked into various areas of microchannel shape to improve the heat transfer rate in microchannel heat sinks. Zhao and Lu (2002) used numerical and analytical methods to investigate the thermal performance of forced convection through a microchannel heat sink. They

determined that when the channel aspect ratio grows, the Nusselt number rises. Ryu et al. (2003) devised a three-dimensional numerical study for improving the thermal performance of an MCHS. They showed that even when the channel number varies significantly, the optimum shape of the geometry remains largely constant. Lee and Garimella (2006) examined convective heat transfer characteristics in microchannels with rectangular cross-sections having different aspect ratios under a constant wall temperature and uniform wall heat flux. They showed that the Nusselt numbers are greatly determined by the axial distance and aspect ratio. Kou et al. (2008) examined the 3D model of MCHS performance numerically by varying the aspect ratio of the channel. They concluded that the optimum width is attained by reducing the height of the channel, which is heavily impacted by the flow velocity. McHale and Garimella (2010) presented thermal characteristics in the trapezoidal microchannels under laminar flow. They reported that altering the channel's aspect ratio influenced the Nusselt number and friction factor. Gunnasegaran et al. (2010) studied the influence of geometry parameters on the thermal performance of microchannels of different shapes. They established that in microchannels with the smallest hydraulic diameter, a high heat transfer coefficient could be achieved.

This paper builds upon the work of Manay et al. (2018) where experimental analysis was carried out on entropy generation of nanofluid in M-shape micro-channel. The current work aim is to conduct three-dimensional numerical analysis on the same microchannel geometry and nanofluid. The objective is to study the influence of geometry and nanfluid, on the heat transfer, fluid flow and entropy generation performance in the M structure microchannel. This micro channel heat sink is novel in the sense that it takes into consideration the pressure losses by chamfering the edges at the inlet as the chamfered edges reduces the pressure losses at the inlet. The results show how the thermal and frictional entropy generation, as well as the entropy generation number ratio, are affected by nanoparticle particle volume fraction and MCHS microchannel height.

2. Materials and methods

2.1 Geometry

The three-dimensional geometry with specified dimensions for the simulation is shown in Fig. 1. The Design Modeler of ANSYS software package was used to create the geometry. The MCHS with a cross-section of length (L), breath (B), and height (t) has a microchannel width B_{ch} and microchannel height H. The four edges at one end of the microchannel heat sink are chamfered with fillet radius (R_B) to reduce the pressure loss that arises at the entrance of the microchannel. The bottom part of the MCHS has three circular slots of radius R_c and length L_c to generate a constant heat flux. The details of the dimensions are shown in Table 1.

2.2 Grid generation (mesh)

The geometry was meshed using ANSYS Mesh. A multi-block mesh generation approach was used, which is based on structured hexahedral meshes (see Fig. 2). The crucial aspect of this study was to monitor as closely as possible the flow and thermal profile around the microchannel; hence, a detailed surface mesh was created for the microchannel region. Further mesh refinement of the geometry was carried out at the model edges and the faces to grasp the flow and thermal field and to ensure accurate results were obtained at the model's periphery and the contact region between the nanofluid and the microchannel. The mesh quality was confirmed by comparing the parameters such as orthogonality, skewness, and aspect ratio to standard values.

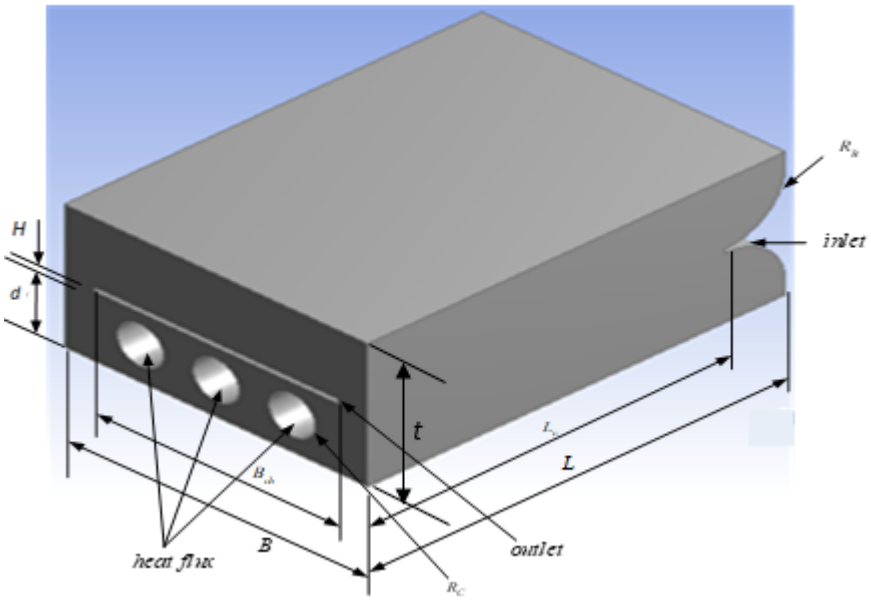

Fig. 1: Geometry of MCHS

Table 1: Geometry parameters

Geometry	Parameter	Dimension
MCHS	L	55mm
	B	40mm
	t	20mm
	d	10mm
	R_B	8mm
Microchannel	B_{ch}	32mm
	H	200μm-500μm
Circular slot	R_c	3mm
	L_c	47mm

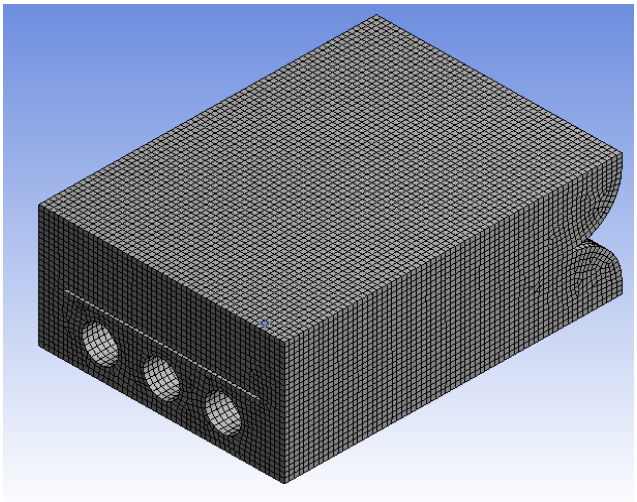

Fig. 2: Multi-block structured grids for the heat sink

2.3 Assumption and governing equations

The assumptions made to simplify the analysis are listed below:

(1) The flow is 3D, incompressible, steady, and laminar.
(2) No-slip at the solid-fluid interface.
(3) The flow is fully developed thermally and hydraulically.
(4) Gravitational, radiation, and magnetic effect are neglected.
(5) Both the fluid and the solid have constant thermophysical characteristics.

The governing equations used in the problem are as follows:

Continuity equation

$$\nabla.\vec{u} = 0 \quad (1)$$

Momentum equation

$$\rho_{nf}(\vec{u}.\nabla)\vec{u} = -\nabla P + \mu_{nf}\nabla^2\vec{u} \quad (2)$$

Energy equation

$$\rho_{nf}Cp_{nf}(\vec{u}.\nabla \mathrm{T}) = k_{nf}\nabla^2 \quad (3)$$

2.4 Boundary conditions

The boundary conditions used in the problem are shown in Table 2.

Table 2: Boundary condition

Boundary	**Location**	**Condition**
	Fluid/solid interface	$u = v = w = 0$
Hydrodynamic	Inlet (MCHS)	$u = U$
	Outlet (MCHS)	$P_{f=1atm}$
Thermal	Fluid/Interface	$-k_s\left(\frac{\partial T_s}{\partial n}\right) = -k_f\left(\frac{\partial T_s}{\partial n}\right)$
	Inlet (MCHS)	$T_{f=}300K, -k_s\left(\frac{\partial T_s}{\partial y}\right) = 0$
	Outlet (MCHS)	$-k_f\left(\frac{\partial T_s}{\partial y}\right) = 0, -k_s\left(\frac{\partial T_s}{\partial y}\right) = 0$
	Circular walls	$80K/Wm^2$
	Top wall (MCHS)	$-k_s\left(\frac{\partial T_s}{\partial y}\right) = 0$
	Bottom wall (MCHS)	$-k_s\left(\frac{\partial T_s}{\partial y}\right) = 0$
	Side Walls (MCHS)	$\frac{\partial}{\partial z} = 0$ (symmetry)

2.5 Nanofluid thermophysical properties

The nanofluid utilized in the studies is TiO_2–water, with a volume fraction of nanoparticles ranging from 0.25 to 2%. The nanofluid thermophysical properties equations are described in Equations (4)-(11) and the computed thermophysical properties of TiO_2-water nanofluid are as shown in Table 3.

Density correlation (Manca et al. 2012)

$$\rho_{nf=}(1-\emptyset)\rho_f + \emptyset\rho_{np} \quad (4)$$

Specific heat correlation (Masoumi et al. 2009)

$$\rho_{nf}Cp_{nf} = (1-\emptyset)Cp_f + \emptyset Cp_{np} \quad (5)$$

Dynamic viscosity

Masoumi et al. (2009) correlation is employed for the effective viscosity, which is a function of the working fluid and nanofluid physical properties.

$$\mu_{nf} = \mu_f + \frac{\rho_{np}V_B d_{np}^2}{72C\delta} \quad (6)$$

where δ is the boundary layer thickness and V_B is Brownian velocity; both could be defined as shown:

$$V_B = \frac{1}{d_{np}}\sqrt{\frac{18K_BT}{\pi\rho_{np}d_{np}}}, \qquad \delta = \sqrt[3]{\frac{\pi}{6\emptyset}}d_{np} \quad (7)$$

$$C = {\mu_f}^{-1}\left[\left(c_1 d_{np} + c_2\right)\emptyset + \left(c_3 d_{np} + c_4\right)\right] \quad (8)$$

where the mean diameter of nanoparticles (d_{np}) is expressed in nanometer, and the constant values ($c_1, c_2, c_3, and\ c_4$) in Equation (8) are defined as:

$c_1 = -0.000001133,\ c_2 = -0.000002771$
$c_3 = 0.00000009,\ c_4 = -0.000000393$ (9)

Thermal conductivity

The Brownian motion and mean diameter of the nanoparticles are utilized to determine the nanofluid effective thermal conductivity, as described by Chon et al. (2005)

$$k_{nf} = k_f\left[164\emptyset^{0.746}\left(\frac{d_f}{d_p}\right)^{0.369}\left(\frac{k_p}{k_f}\right)^{0.746} {Pr_{nf}}^{0.9955}{Re_{nf}}^{1.2321}\right] \quad (10)$$

where Pr_{nf} and Re_{nf} are expressed as:

$$Pr_{nf} = \frac{\mu_{nf}}{\rho_{nf}\alpha_{nf}}, \qquad Re_{nf} = \frac{\rho_{nf}\,k_B T}{3\pi\mu_{nf}^2 l_{mf}}, \qquad K_B = 1.3807e^{-23} \quad (11)$$

l_{mf} represents the mean free path of the base fluid, K_B denotes Boltzmann constant.

Table 2: The computed Thermo-physical properties of TiO_2-water nanofluid from the above-mentioned equations based on the mean diameter of 5nm

$\emptyset(\%)$	$\rho(kg/m^3)$	$\mu(Pa.s)$	$C_p(J/kgK)$	$k(W/mk)$
0	997	0.001003	4182.00	0.600000
0.25	1004.258	0.001016	4173.32	0.627962
0.5	1011.515	0.001023	4164.64	0.626457
1.0	1026.030	0.001038	4147.28	0.625007
1.5	1040.545	0.001053	4129.92	0.624198
2.0	1055.060	0.001067	4112.56	0.623651

2.6 Entropy generation analysis

Entropy generation analysis was incorporated to account for fluid flow and heat transfer irreversibility in the heat sink, and the irreversibility is a result of $\dot{S}'_{gen\,th}$ and $\dot{S}'_{gen\,fr}$. The total entropy generation rate is expressed as:

$$\dot{S}'_{gen} = \dot{S}'_{gen\,th} + \dot{S}'_{gen\,fr} \quad (12)$$

where $\dot{S}'_{gen\,th}$ and $\dot{S}'_{gen\,th}$ are solved by Equations (13) and (14), respectively:

$$\dot{S}'_{gen\,th} = \frac{\lambda_f}{T_f^2}\left[\left(\frac{\partial T}{\partial x}\right)^2 + \left(\frac{\partial T}{\partial y}\right)^2 + \left(\frac{\partial T}{\partial z}\right)^2\right] \quad (13)$$

$$\dot{S}'_{gen\,fr} = \frac{\mu}{T_f}\left\{2\left[\left(\frac{\partial u}{\partial x}\right)^2 + \left(\frac{\partial v}{\partial y}\right)^2 + \left(\frac{\partial w}{\partial z}\right)^2\right] + \left(\frac{\partial u}{\partial y} + \frac{\partial v}{\partial x}\right)^2 + \left(\frac{\partial u}{\partial z} + \frac{\partial w}{\partial x}\right)^2 + \left(\frac{\partial v}{\partial z} + \frac{\partial w}{\partial y}\right)^2\right\} \quad (14)$$

The velocity components in the x, y, and z directions are denoted by u, v, and w, respectively. Equations (13) and (14) were integrated to obtain:

$$\dot{S}'_{gen\,th} = \frac{q'^2\pi D_h^2}{KT^2Nu} \quad (15)$$

$$\dot{S}'_{gen\,th} = \frac{8\dot{m}^3 f}{\pi^2\rho^2 T D_h^5} \quad (16)$$

$$Re = \frac{\rho_{nf} U D_h}{\mu_{nf}} \quad (17)$$

$$f = \frac{\nabla P D_h}{2\rho U^2 l} \quad (18)$$

The entropy generation number (N_s) is represented as:

$$N_s = \frac{\dot{S}'_{gen}}{\dot{S}'_{gen\,o}} \quad (19)$$

where $\dot{S}'_{gen\,o}$ denotes the baseline total entropy generation rate.

2.7 Numerical procedure

All the equations, including the continuity, Navier-Stokes, heat transfer equations, and the respective boundary conditions were solved using ANSYS (FLUENT) commercial code based on the finite volume method. The SIMPLEC (Semi-Implicit Method for Pressure Linked Equations-Consistent) algorithm was selected for pressure-velocity coupling. For the discretization scheme, the Least Squares Cell-based was chosen for the gradient and Second-Order Upwind was set for pressure, momentum, and energy equation. However, the convergence tolerance of 10^{-6} was set for all the equations.

3. Results and discussion

3.1 Grid independence test and validation

A grid sensitivity analysis has been conducted to effectively optimize the number of grids and save computational costs. Seven different mesh

sizes (Table 4), represented by M_1, M_2, M_3, M_4, M_5, M_6, and M_7 arranged according to their increasing number of elements and nodes, have been considered. Fig. 3 shows the grid independence test; it compares the Nu at different mesh sizes for the case of microchannel height of 0.5mm and 2% volume of nanoparticles at Reynold number of 800. It was observed that refining the grid from M_5 to M_7 does not change the results (considering four decimal digits) in any of the cases. Therefore, the M_5 grid was used to simulate all other results.

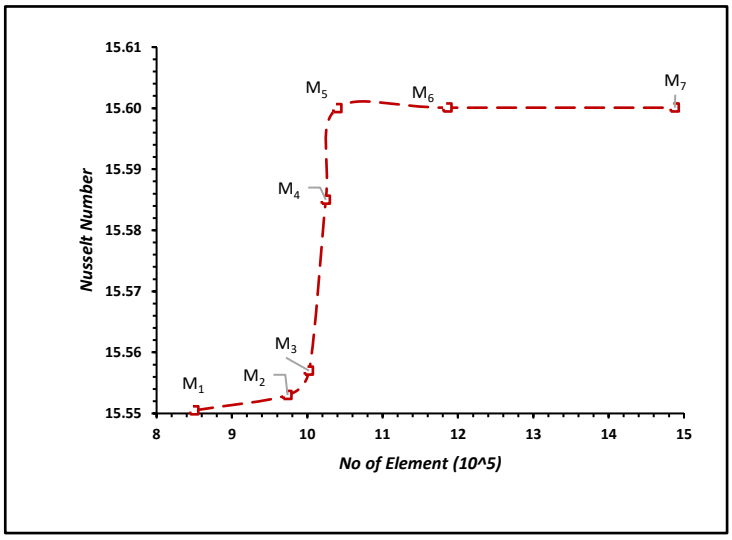

Fig. 3: Grid independence test

Table 4: Mesh Independence test result comparing Nusselt Number for different meshes for H=0.5mm, $\emptyset = 2\%, Re = 800$

Mesh	No of Elements	No of Nodes	Nusselt Number
Mesh 1	850012	196003	15.55050
Mesh 2	973874	198132	15.55300
Mesh 3	1002403	199725	15.55700
Mesh 5	1024610	201432	15.58500
Mesh 5	1039937	202483	15.60000
Mesh 6	1186421	204311	15.60008
Mesh 7	1487901	205342	15.60008

3.2 Validation and verification

The numerical results of this study were verified with correlations published in the literature. A geometry similar to the one used for the experimental work of Manay et al. (2018) was considered for the validation as shown in Fig. 4. The present friction factor results are consistent with the experimental results of Manay et al. (2018) but have lower values than the experimental results of Kandlikar and Grande (2004). The Nusselt number results of our investigation, as shown in Fig. 4, are extremely close to the experimental results of Manay et al. (2018) and Shah and London (1978). Nonetheless, they show a substantial difference from the experimental work of Teng et al. (2010). This favourable comparison confirms that the current numerical model is accurate.

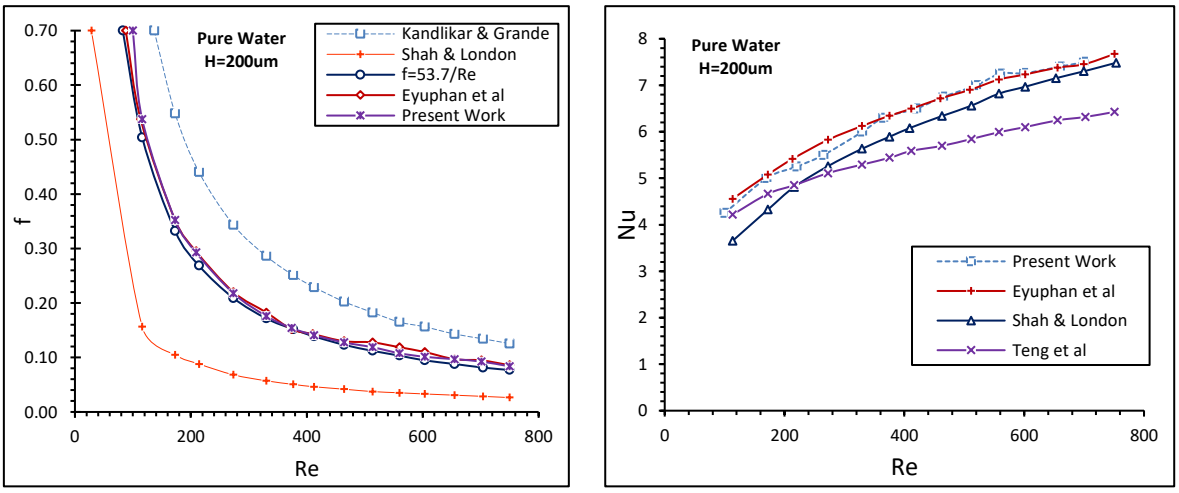

(a) (b)

Fig. 4: The comparison of present study (a). friction factor and (b). Nusselt number results with the existing experimental correlations in the literature

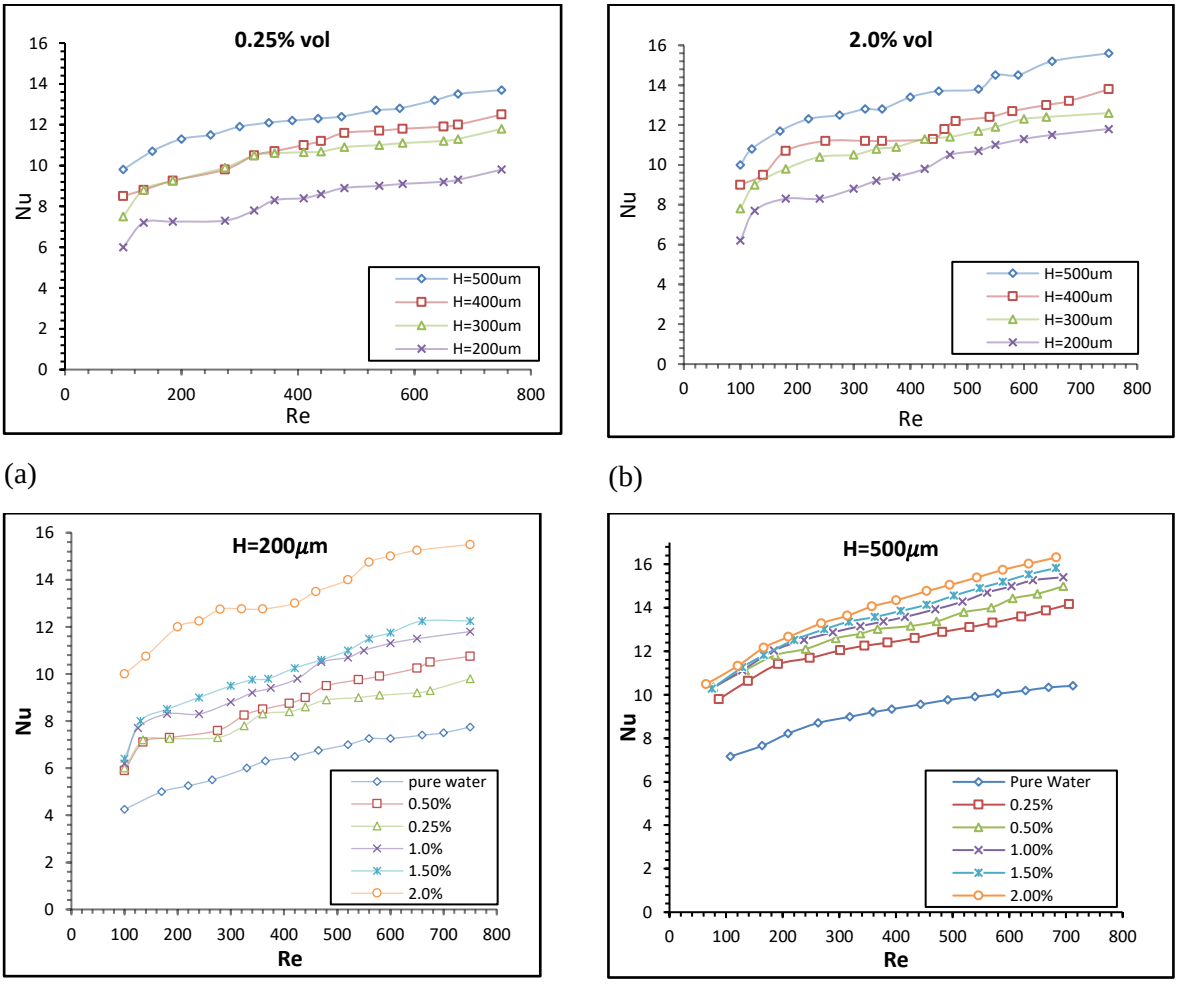

(a) (b)

(c) (d)

Fig. 5: Comparison of Nusselt number against Reynold number for (a). Ø=0.25% (b). Ø=2.0% (c). H=200 μm (d). H=500 μm

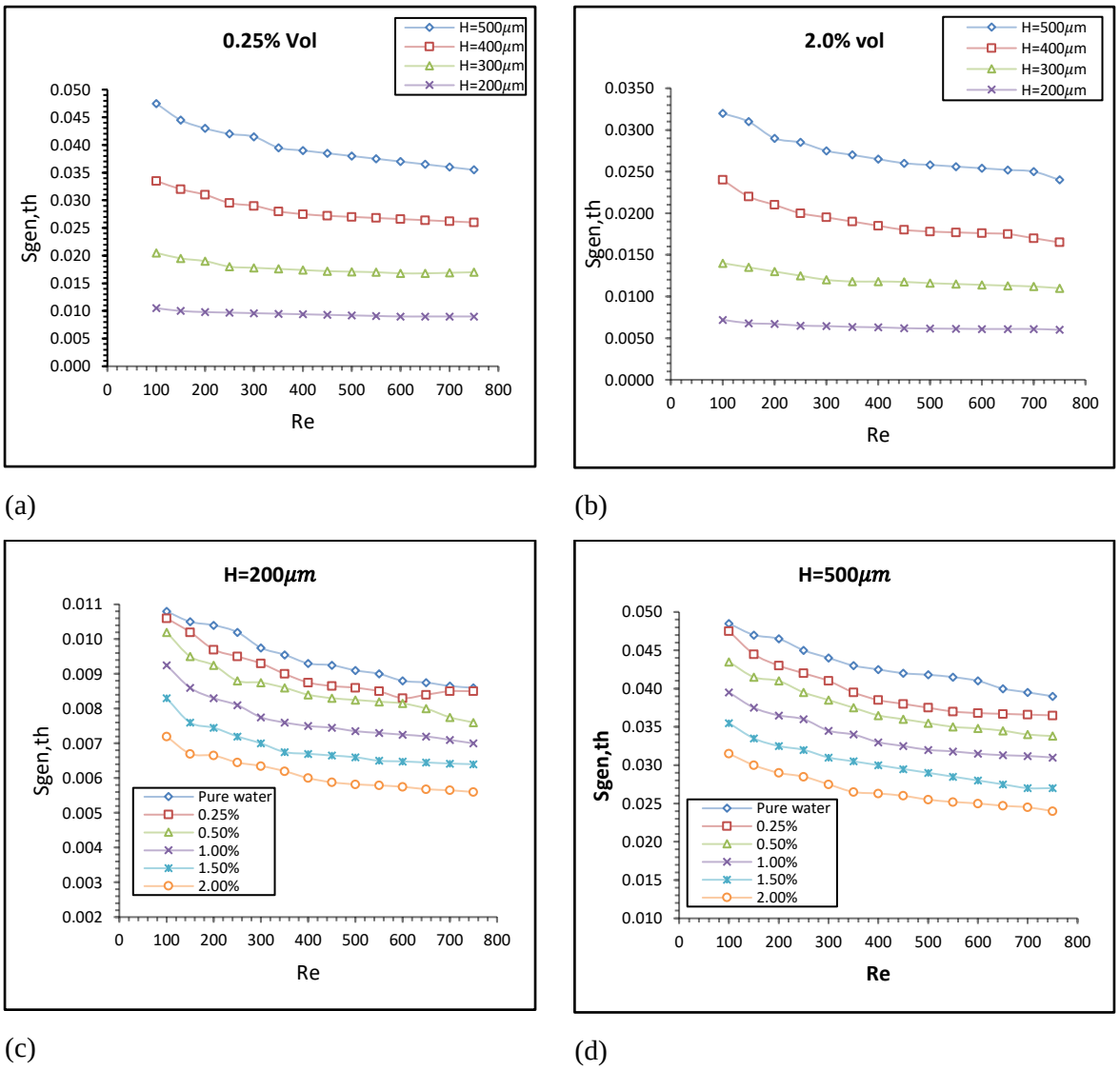

(a) (b)

(c) (d)

Fig. 6: $\dot{S}'_{gen,th}$ vs. Re for (a). Ø=0.25% (b). Ø=2.0% (c). H=200μm (d). H=500 μm

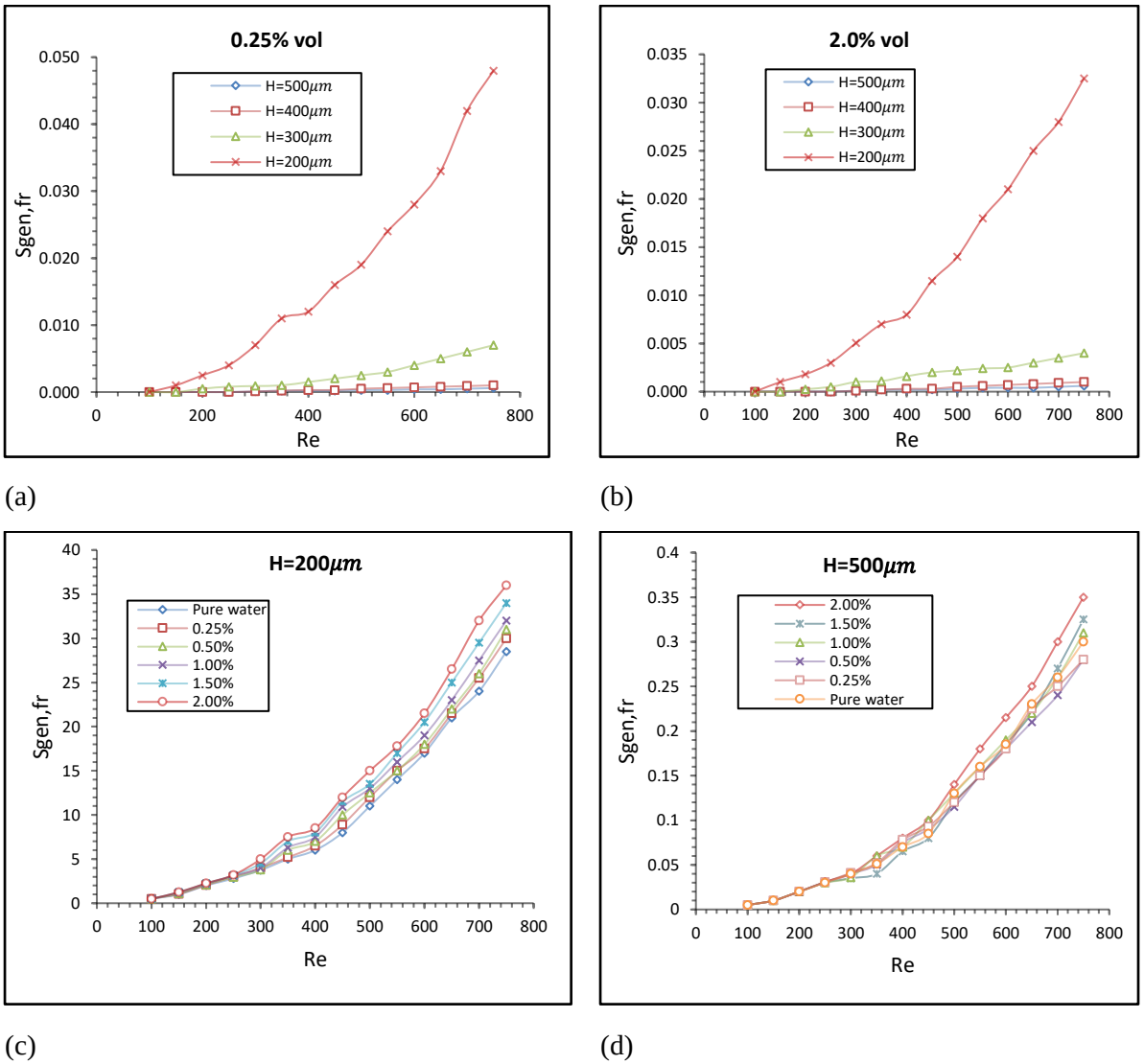

Fig. 7: $\dot{S}_{gen,fr}$ vs. Re for (a). Ø=0.25% (b). Ø=2.0% (c). H=200μm (d). H=500 μm

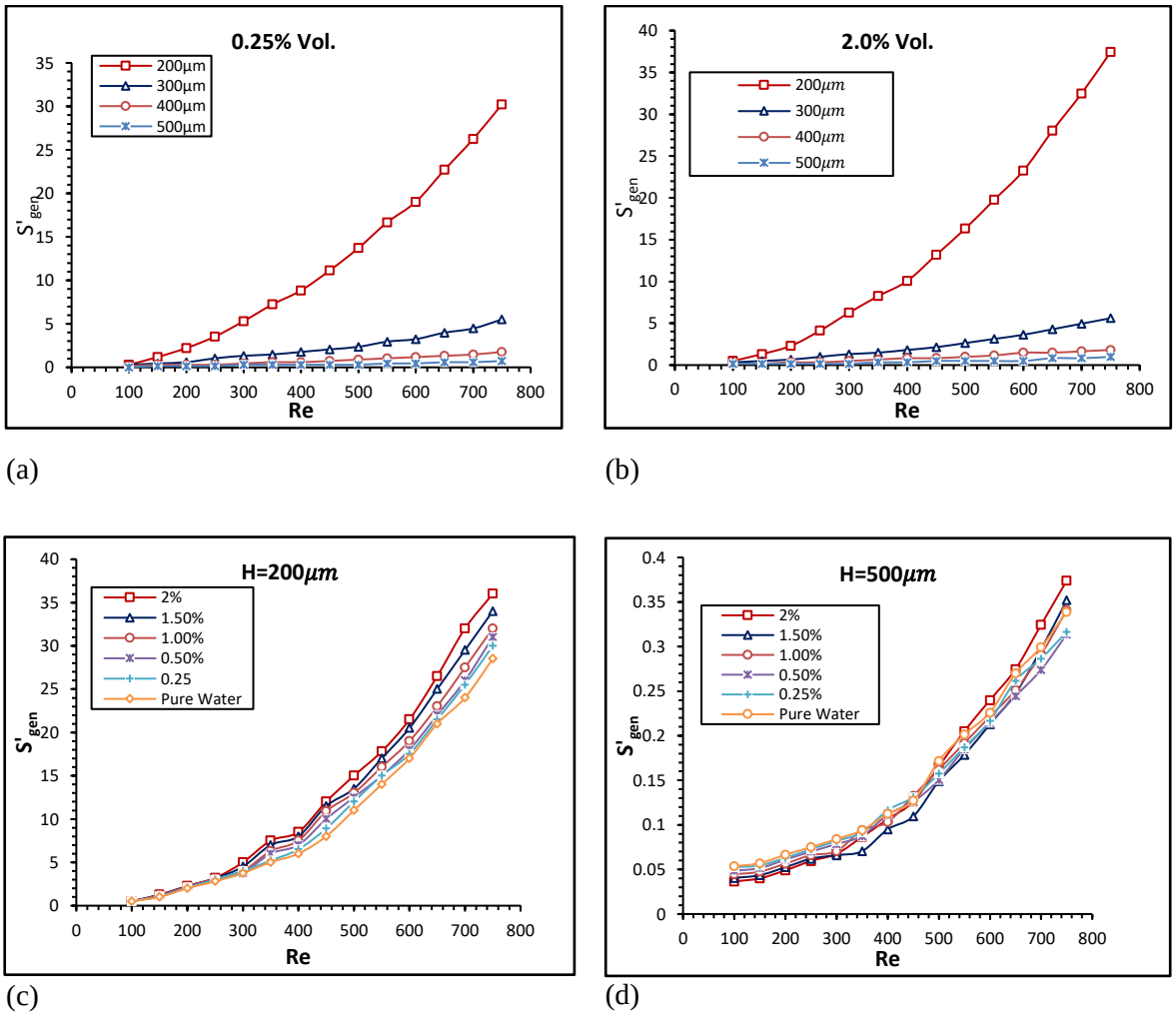

(a) (b)

(c) (d)

Fig. 8: $\dot{S}'_{gen}$ vs. Re for (a). Ø=0.25% (b). Ø=2.0% (c). H= 200μm (d). H= 500 μm

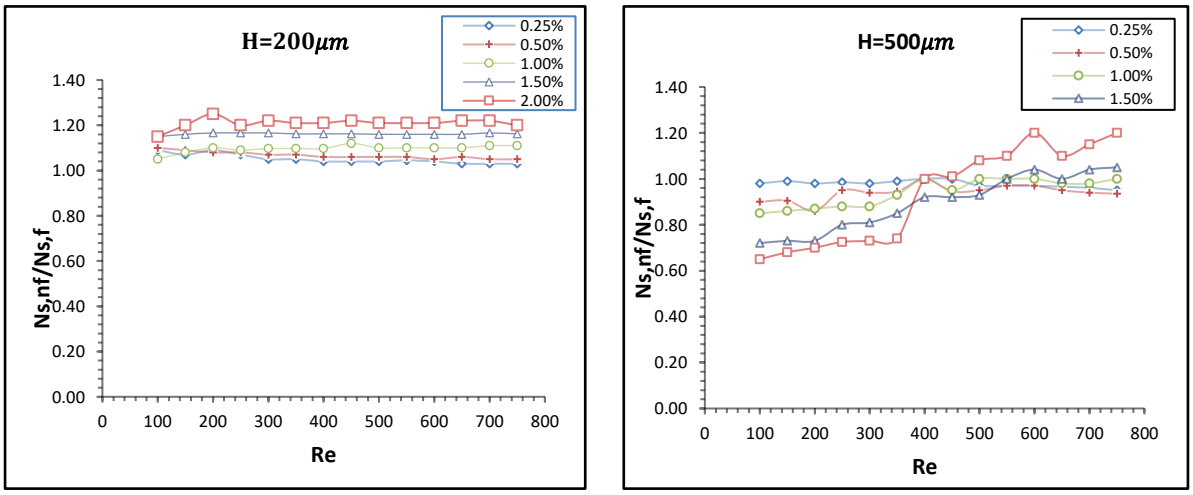

(a) (b)

Fig. 9: $N_{s,nf}/N_{s,f}$ vs Re for (a). H= 200μm (b). H= 500 μm

Fig. 5a through Fig. 5d illustrate the variations of the Nu against the Re for the nanoparticle volume fraction ($\emptyset$) of 0.25% and 2%, and microchannel height (H) of 200μm and 500μm. It was observed that as the Nu increases, the Re increases for all the cases studied. For all $\emptyset$, it was revealed that Nu increases with increases in $\emptyset$, but lower Nu was recorded for pure water. This is because an increase in $\emptyset$ enhances the thermal conductivity of nanofluid while dynamic viscosity increases and specific heat decreases. However, the higher value of the Nu is obtained as H is increased. Increasing H from 200μm to 500 μm yields an increase in Nu of about 6.77%-57%, and increasing the $\emptyset$ of nanoparticles from 0.25% to 2% causes an enhancement in heat transfer from 30%-98.9%.

Fig. 6a through Fig. 6d demonstrate the relationship between the $S'_{gen,th}$ and the Re for $\emptyset$ ranging from 0.25% to 2% and H ranging from 200μm to 500μm. As shown in Fig. 6a–b, the thermal entropy generation rate reduces as the Reynolds number increases. More so, a 0.25%–2.0% increment in the nanoparticles volume fraction reduces the thermal entropy generation rate value by 1.85%-33.3% as compared to pure water. The reason for this is that the thermal conductivity of pure water is greatly influenced by the addition of nanoparticles. Thus, thermal performance is improved at the larger nanoparticle volume fraction, and flow resistance is decreased, which in turn reduces the thermally generated entropy. It was found that the $\dot{S}'_{gen\,th}$ for H= 500μm is about 4.5 times higher than that of H= 200μm. As seen in Figure 6c-d, $\dot{S}'_{gen\,th}$ declines as microchannel height reduces. By reducing H from 500μm to 200μm, $\dot{S}'_{gen\,th}$ reduces by 77.5%-26.8% and vice-versa. However, the $\dot{S}'_{gen\,th}$ for $\emptyset$=0.25% is approximately 1.5 times that of $\emptyset$=2%.

Fig. 7a through 7d present the relationship between the $\dot{S}'_{gen\,fr}$ and Re for the $\emptyset$ ranging from 0.25% to 2%, and H ranging from 200μm to 500μm. As demonstrated in Fig. 7a-b, considering the H, $\dot{S}'_{gen}$ due to friction factor increases with Re. The highest value of $\dot{S}'_{gen\,fr}$ was obtained when H =200μm while the least was obtained when H =500μm. Decreasing the H of a heat sink increases the degree of irreversibility since pressure drop in the microchannel increased with Re due to the blockage effect. Under a varied H both volume fractions of 0.25% and 2% show a similar behavior across all microchannel heights. A more remarkable change in $\dot{S}'_{gen\,fr}$ occurs by reducing H from 300μm to 200μm. Overall, reducing the H from 500μm to 200μm causes a 75%-99% increment in the $\dot{S}'_{gen\,fr}$. The results show that $\dot{S}'_{gen\,fr}$ for $\emptyset$=0.25% is approximately 1.5 times that of $\emptyset$=2%.

From Fig. 7c-d, at a fixed $\emptyset$, $\dot{S}'_{gen\,fr}$ increases with an increase in Re. As the $\emptyset$ rises, the rate of $\dot{S}'_{gen\,fr}$ increases. The highest value of $\dot{S}'_{gen\,fr}$ was obtained when the volume fraction is 2.0%, while the lowest $\dot{S}'_{gen\,fr}$ value occurred in pure water. This is because nanofluid becomes more viscous by adding nanoparticles. No significant change in the rate of $\dot{S}'_{gen\,fr}$ was observed in all volume fractions at $Re < 280$, which implies no appreciable pressure drop is evident. As Re increases from 280, the difference in $\dot{S}'_{gen\,fr}$ in all the $\emptyset$ becomes more and more significant. $\dot{S}'_{gen\,fr}$ for $H = 500\mu m$ is approximately 103 times that of $H = 200\mu m$. By increasing $\emptyset$ from 0.25%-2%, frictional entropy increased in value by 2.22%–26.5% as compared to pure water.

Fig. 8a-d presents the comparison of the total entropy generation rate ($\dot{S}'_{gen}$) with Re for $\emptyset$ ranging from 0.25% to 2%, and H ranging from 200μm to 500μm. The $\dot{S}'_{gen}$ increases as H_{ch} decreases, and both Re and volume fraction increase. As illustrated in Figure 8c-d, increasing $\emptyset$ from 0.25% to 2% causes the $\dot{S}'_{gen}$ to increase from 5% to 26%. More so, the $\dot{S}'_{gen}$ for H=200μm is approximately 96 times that of H=500μm. As presented in Figure 8a-b, for $\emptyset$=0.25% and $\emptyset$=2%, the $\dot{S}'_{gen}$ increases from 58% to 97% as H decreases from 500μm to 200μm. In addition, $\dot{S}'_{gen}$ for $\emptyset$=2% is approximately 1.3 times higher than $\emptyset$=0.25%.

Fig. 9a-b reveals the entropy generation number ratio ($N_{s,nf}/N_{s,f}$) as a function of Re for $\emptyset$ ranging from 0.25% to 2% and H ranging from 200μm to 500μm. The $N_{s,nf}/N_{s,f}$ is one of the yardsticks to measure the optimum overall performance of the microchannel. When $N_{s,nf}/N_{s,f}$ is smaller than 1, it means that the heat sink has a better overall performance. As illustrated in Fig. 9a, considering the impact of nanoparticle volume fraction ($\emptyset$), $N_{s,nf}/N_{s,f}$ rises with volume fraction for H of 200μm. The highest value of $N_{s,nf}/N_{s,f}$ was obtained in the 2% volume fraction nanofluid, while the lowest value was obtained in the 0.25% volume fraction nanofluid. In addition, all volume

fractions (0.25%-2%) exhibit $N_{s,nf}/N_{s,f}$ greater than unity. As shown in Fig. 9b, considering H =500μm, for $0 \leq Re \leq 400$, each $\emptyset$ depicts $N_{s,nf}/N_{s,f}$ less than unity. For $400 < Re \leq 750$, all $\emptyset$ exhibit an $N_{s,nf}/N_{s,f}$ greater than unity, which means that adopting a nanofluid at this range of Re is not advisable.

4. Conclusion

In the present work, heat transfer improvement of M-like structured MCHS due to entropy generation of TiO_2 nanofluid at various $\emptyset$ and H was numerically examined. The objectives of this paper are mainly threefold which are: first, to investigate the effects of $\emptyset$ on Nu, $\dot{S}'_{gen\,th}$ and $\dot{S}'_{gen\,fr}$. Second, to investigate the effects of H on Nu, $\dot{S}'_{gen\,th}$ and $\dot{S}'_{gen\,fr}$. Lastly, to determine the influence of $\emptyset$ and H on $N_{s,nf}/N_{s,f}$. The findings for the present work are summarized as follows:

1. As Re increased, Nu, $\dot{S}'_{gen\,fr}$, and $\dot{S}'_{gen}$ increased, whereas $\dot{S}'_{gen\,fr}$ dropped.
2. For all H increasing $\emptyset$ caused the Nu, $\dot{S}'_{gen\,fr}$, and $\dot{S}'_{gen}$ to rise, and thermal irreversibility decreased. The highest values of $\dot{S}'_{gen\,fr}$, $\dot{S}'_{gen}$ and Nu were achieved at $\emptyset$=2%, while the reverse was the case of thermal irreversibility. Therefore, incorporating TiO_2 nanoparticles into the pure water or an existing nanofluid improved the thermal performance of the MCHS.
3. For all $\emptyset$, the Nu and rate of the entropy production increased, whereas frictional and total entropy production rate decreased with increasing microchannel height. At $H = 500\mu m$, the maximum Nusselt number and rate of thermal entropy generation were obtained, but the reverse was the case for the frictional and rate of total entropy generation.
4. For $H = 200\mu m$, the $N_{s,nf}/N_{s,f}$ was greater than unity at all given Re. For the case of H =500μm, the $N_{s,nf}/N_{s,f}$ was less than one when $Re \leq 400$.

References

Bianco V., Manca, O. and Nardini S. (2014) Performance analysis of turbulent convection heat transfer of Al_2O_3 water-nanofluid in circular tubes at constant wall temperature. Energy, 77:403-13.

Cengel Y.A., and Boles, M.A. (2011) Thermodynamics: an engineering approach. New York: McGraw-hill. p. 930.

Chein, R. and Hunag, G. (2005) Analysis of microchannel heat sink performance using nanofluids. Applied Thermal Engineering, 25: 3104-3114.

Chein, R. and Chuang, J. (2007) Experimental microchannel heat sink performance studies using nanofluids. International Journal of Thermal Sciences, 46:5-66.

Chon, C.H., Kihm, K.D., Lee, S.P., and Choi, S. (2005) Empirical correlation finding the role of temperature and particle size for nanofluid (Al_2O_3) thermal conductivity enhancement. Applied Physics Letters, 87:1-3.

Choi, S.U.S. and Eastman, J.A. (1995). Enhancing thermal conductivity of fluid with nanoparticles. ASME International Mechanical Engineering Congress & Exhibition, San Francisco, CA.

Choi, S.U. (1995). Enhancing thermal conductivity of fluids with nanoparticles. ASME FED, 231:99-103.

Choi, S.U.S., Zhang, Z.G., Yu, W., Lockwood, F.E. and Grulke, E.A. (2001) Anomalous thermal conductivity enhancement in nanotube suspensions. Applied Physics Letters, 79(14): 2252-2254.

Das, S.K., Putra, N., Theisen, P. and Roetzel, W. (2003) Temperature dependence of thermal conductivity enhancement for nanofluid. Journal of Heat Transfer, 125:567-574.

Ebrahimi, A., Rikhtegar, F., Sabaghan, A. and Roohi, E. (2016) Heat transfer and entropy generation in a microchannel with longitudinal vortex generators using nanofluids. Energy, 101:190-201.

Gunasegaram, P., Mohammed, H.A., Shuaib, N.H. and Saidur R. (2010) The effect of geometrical parameters on heat transfer characteristics of microchannels heat sink with different shapes. International Communication of Heat Mass Transfer, 37:1078-1086.

Hassan, M., Sadri, R., Ahmadi, G., Dahari, M.B., Kazi, S, N., Safaei, M.R. and Sadeghinezhad, E. (2013) Numerical study of entropy generation in a flowing nanofluid used in micro and minichannels. Entropy, 5:144-55

Ho, C.J., Chen, M. and Li, Z. (2008) Numerical Simulation of Natural Convection of Nanofluid in a Square Enclosure: Effects due to Uncertainties of Viscosity and Thermal

Conductivity. International Journal of Heat and Mass, 51(17):4506-4516

Ibáñez, G., López, A., Pantoja, J., Moreira, J. and Reyes, J.A. (2013) Optimum slip flow based on the minimization of entropy generation in parallel plate microchannels. Energy, 50:143-149.

Jang, S.P. and Choi, S.U.S. (2006) Cooling performance of a microchannel heat sink with nanofluids. Applied Thermal Engineering, 26: 2457-2463.

Kandlikar, S.G., and Grande, W.J. (2004) Evaluation of single-phase flow in microchannels for high heat flux chip cooling-thermo hydraulic performance enhancement and fabrication technology. Heat Transfer Eng, 25(8):5-16.

Koo, J. and Kleinstreuer, C. (2005) Laminar nanofluid flow in micro-heatsinks. International Journal of Heat and Mass Transfer, 48:2652-2661.

Kou, H.S., Lee J.J. and Chen C.W. (2008) Optimum thermal performance of microchannel heat sink by adjusting channel width and height. Int. Commun. Heat Mass Transfer, 35:577-582.

Lee, P.S. and Garimella, S.V. (2006) Thermally developing flow and heat transfer in rectangular microchannels of different aspect ratios, Int. J. Heat Mass Transfer. 49:3060-3067.

Lee, S., Choi, S.U., Li, S. and Eastman, J.A. (1999) Measuring thermal conductivity of fluids containing oxide nanoparticles. Journal of Heat Transfer, 121:280-289.

Li, P., Zhang, D. and Xie, Y. (2014) Heat Transfer and Flow Analysis of Al2O3–Water Nanofluids in Microchannel with Dimple and Protrusion. Int. J. Heat. Mass. Tran., 73:456-467.

Manay, E., Akyurek, E.F., and Sahin, B. (2018) Entropy generation of nanofluid flow in a microchannel heat sink. J. Results in Physics, 9: 615-624.

Manca, O., Nardini, S., Ricci, D. and Tamburrino, S. (2012) Numerical Investigation on Mixed Convection in Triangular Cross-Section Ducts with Nanofluids. Adv. Mech. Eng., 4:139370.

Masoumi, N., Sohrabi, N. and Behzadmehr, A. (2009) A new model for calculating the effective viscosity of nanofluids. J. Phys. D Appl. 42(5):055501.

McHale, J.P. and Garimella, S.V. (2010). Heat transfer in trapezoidal microchannels of various aspect ratios. Int. J. Heat Mass Transfer, 53: 365-375.

Park, H.S. and Punch, J. (2008) Friction factor and heat transfer in multiple microchannels with uniform flow distribution. Int J Heat Mass Transfer, 51:4535-43.

Roy, G., Nguyen, C.T. and Lajoie, P, R. (2004) Numerical Investigation of Laminar Flow and Heat Transfer in a Radial Flow Cooling System with the Use of Nanofluids. Super Lattices Microstructure. 35(3):497-511.

Ryu, J.H., Choi D.H. and Kim S.J. (2003). Three-dimensional numerical optimization of a manifold microchannel heat sink. Int. J. Heat Mass Transfer, 46:1553-1562.

Shalchi, T.A. and Seyf, H.R. (2012) Analysis of entropy generation and convective heat transfer of Al_2O_3 nanofluid flow in a tangential micro heat sink. Int J Heat Mass Transf, 55(16):366-375.

Shah, R.K. and London, A.L. (1978) Laminar flow forced convection in ducts. J. Fluids Eng. 102(2):431-455.

Sohel, M.R., Saidur, R., Hassan, N.H., Elias, M.M., Khaleduzzaman, S.S. and Mahbubul, I.M. (2013) Analysis of entropy generation using nanofluid flow through the circular microchannel and mini-channel heat sink. Int Commun Heat Mass Transf, 46:85-91.

Teng, T.P., Hung, Y., Teng, T.C., Moa, H.E. and Hsu, H, G. (2010) The effect of alumina/water nanofluid particle size on thermal conductivity. Appl. Therm. Eng., 30:213-218.

Ting, T.W., Hung, Y.W. and Guo, N. (2016) Viscous dissipation effect on streamwise entropy generation of nanofluid flow in microchannel heat sinks. J Energy Resource Technol. 138:1-9.

Tuckerman, D.B. and Pease, R.F. (1981) High-performance heat sinking for VLSI. IEEE Electronic Devices Letters EDL 2, 126–129.

Vajjha, R.S., and Das, D.K. (2009) Experimental determination of thermal conductivity of three nanofluids and development of new correlations. International Journal of Heat and Mass Transfer, 52(21-22):4675-4682.

Yang, Y., Zhang, Z., Grulke, E.A. and Anderson, W.B. (2005) Heat transfer properties of nanoparticle in fluid dispersions (nanofluids) in laminar flow. International Journal of Heat and Mass Transfer, 48:1107-1116.

Zhao, C.Y. and Lu, T.J. (2002) Analysis of microchannel heat sinks for electronics cooling. Int. J. Heat Mass Transfer, 45:4857-4869.